Kurdish Studies
August 2024
Volume: 12, No: 2, pp 7104 - 7115
ISSN: 2051-4883 (Print) | ISSN 2051-4891 (Online)
www.KurdishStudies.net

DOI: 10.69980/ks.v12i2.4118

Synthesis and characterization of phytocompound loaded metallic nanoparticles for the treatment of HAPE

Iqra Sharif*[1], Asma Ahmed[1], Aliza Rafique[2]
[1*]Institute of Molecular Biology and Biotechnology, The University of Lahore, Lahore, Pakistan, Email: iqra.sharif@yahoo.com
[1*]Institute of Molecular Biology and Biotechnology, The University of Lahore, Lahore, Pakistan,
[2]Department of Biological Sciences, Superior University Lahore, Pakistan

Abstract
High Altitude Pulmonary Edema (HAPE) is a life-threatening, non-cardiogenic pulmonary disorder caused by hypobaric hypoxia at high altitudes, leading to pulmonary hypertension, endothelial dysfunction, oxidative stress, and fluid accumulation in the lungs. Despite available therapeutic interventions, effective site-specific drug delivery remains a significant challenge due to poor bioavailability and systemic side effects. Nanotechnology-based drug delivery systems, particularly zinc oxide (ZnO) nanoparticles, offer a promising approach to improve drug stability, controlled release, and targeted delivery. Owing to their biocompatibility, large surface area, and ease of surface functionalization, ZnO nanoparticles have gained considerable attention as potential nanocarriers for pulmonary therapeutics. The present study aimed to synthesize ZnO nanoparticles through a green approach using P. roxburghii (L.) Sarg. leaf extract and develop a ZnO-based nanocomposite loaded with the bioactive compound 2-Propanone, 1-hydroxy-3-(4-hydroxy-3-methoxyphenyl) as a potential targeted drug delivery system for HAPE. The nanoparticles were synthesized using the aqueous leaf extract as a natural reducing and stabilizing agent, followed by loading of the selected bioactive compound. The synthesized materials were characterized using UV–Visible spectroscopy, Fourier Transform Infrared Spectroscopy (FTIR), X-ray Diffraction (XRD), Scanning Electron Microscopy (SEM), and Energy Dispersive X-ray Spectroscopy (EDX). The UV–Visible spectrum showed a characteristic absorption peak at 377 nm, confirming ZnO nanoparticle formation. FTIR analysis demonstrated the involvement of phytochemicals in nanoparticle synthesis and verified successful loading of the bioactive compound through changes in characteristic functional group vibrations. XRD confirmed the crystalline hexagonal wurtzite structure of ZnO nanoparticles, while SEM revealed irregularly shaped particles with an average size of 24.71 nm. EDX analysis confirmed zinc and oxygen as the predominant elemental constituents, indicating the successful synthesis of high-purity ZnO nanoparticles. Overall, the findings demonstrate the successful green synthesis and characterization of a ZnO nanocomposite with desirable physicochemical properties. This nanocomposite represents a promising platform for targeted drug delivery, providing a foundation for future biological and pharmacological studies to evaluate its therapeutic potential in the management of High-Altitude Pulmonary Edema.

Keywords: High Altitude Pulmonary Edema (HAPE); Zinc Oxide Nanoparticles (ZnO NPs); Green Synthesis; Pinus roxburghii; Targeted Drug Delivery; Nanocomposite

Introduction

When normally healthy people rapidly ascend to high elevations, usually above 2,500 meters, they may develop high-altitude pulmonary edema (HAPE), a severe and potentially fatal form of non-cardiogenic pulmonary edema (Bartsch & Swenson, 2013). Excessive fluid buildup in the lungs' alveolar gaps causes respiratory discomfort, severe hypoxemia, poor gas exchange, and, if left untreated, death. HAPE continues to be one of the most dangerous altitude-related illnesses that affects hikers, climbers, military personnel, and those who live or travel in mountainous areas. The pathophysiological complexity of HAPE continues to present major obstacles for efficient clinical care, despite advancements in preventive and therapeutic approaches (Maggiorini, 2006).

Exposure to hypobaric hypoxia at high altitudes is the main cause of HAPE. When atmospheric pressure drops, less oxygen is available, which triggers a number of physiological reactions meant to keep tissue oxygenation at a sufficient level. However, hypoxia causes excessive hypoxic pulmonary vasoconstriction (HPV) in vulnerable people, which raises pulmonary arterial pressure and causes irregular pulmonary blood flow. The alveolar-capillary barrier is mechanically stressed by the elevated hydrostatic pressure inside pulmonary capillaries, which results in fluid leaking into the alveolar spaces and pulmonary edema (Swenson &Bärtsch, 2012; West et al., 2011).

New research indicates that oxidative stress and inflammation are important factors in the development of HAPE, in addition to hemodynamic changes. Reactive oxygen species (ROS) are produced in excess in hypoxic conditions, which damages cells and compromises endothelium integrity (Sartori et al., 2002). Moreover, elevated expression of inflammatory mediators such as vascular endothelial growth factor (VEGF), interleukin-6 (IL-6), and tumor necrosis factor-alpha (TNF-α) leads to increased vascular permeability and edema development. Together, these molecular processes worsen lung damage and impair breathing (Bailey et al., 2009).

Improving oxygenation and lowering pulmonary hypertension are the main goals of current HAPE treatment strategies. Supplemental oxygen therapy, descent to lower altitudes, portable hyperbaric chambers, and pharmaceuticals such dexamethasone, phosphodiesterase inhibitors, and nifedipine are examples of standard interventions. Despite their potential effectiveness, these treatments have a number of drawbacks, such as a delayed beginning of action, systemic adverse effects, low target specificity, and limited accessibility in isolated high-altitude settings. As a result, there is a growing demand for novel treatment approaches that can more successfully target the underlying pathophysiological mechanisms of HAPE (Luks et al., 2019; Stream & Grissom, 2008).

A promising multidisciplinary field, nanotechnology has the potential to significantly improve lung disease diagnosis, prevention, and therapy. High surface area, better bioavailability, controlled drug release, and improved cellular absorption are just a few of the distinctive physicochemical characteristics of nanoparticles, which are nanoscale objects with sizes typically between 1 and 100 nanometers. Because of these qualities, nanoparticles are appealing options for targeted drug delivery systems, especially in respiratory conditions where localized therapy can improve therapeutic efficacy while reducing systemic toxicity (Patra et al., 2018; Ventola, 2017).

The potential of nanoparticle-based drug delivery systems to get beyond the drawbacks of traditional therapies has drawn a lot of attention in recent years. By delivering therapeutic drugs straight to the lungs, nanoparticles can be designed to increase medication concentration at the site of injury while minimizing negative systemic effects. Numerous nanocarriers have shown great promise in pulmonary drug delivery applications, including polymeric nanoparticles, liposomes, solid lipid nanoparticles, metallic nanoparticles, and nanostructured lipid carriers. They are especially useful for treating complex pulmonary disorders like HAPE because of their capacity to cross biological barriers and induce sustained drug release (Muralidharan et al., 2015; Paranjpe& Müller-Goymann, 2014).

In recent years, there has been a lot of interest in the possibility of drug delivery systems based on nanoparticles to overcome the limitations of conventional medicines. Nanoparticles can be engineered to enhance medicine concentration at the site of injury while reducing adverse systemic effects by delivering therapeutic medications directly to the lungs. Polymeric nanoparticles, liposomes, solid lipid nanoparticles, metallic nanoparticles, and nanostructured lipid carriers are just a few of the nanocarriers that have demonstrated significant promise in pulmonary drug delivery applications. Their ability to overcome biological barriers and generate continuous drug release makes them particularly helpful for treating complex pulmonary illnesses such as HAPE (Muralidharan et al., 2015; Paranjpe & Müller-Goymann, 2014).

Metallic nanoparticles have demonstrated exceptional therapeutic promise among the various nanomaterials studied because of their targeted delivery, anti-inflammatory, and antioxidant qualities. The ability of zinc oxide, gold, silver, and iron oxide nanoparticles to alter inflammatory reactions and oxidative stress pathways has been thoroughly investigated. Because zinc is a necessary trace element involved in immunological control, cellular communication, antioxidant defense mechanisms, and endothelial function maintenance, zinc-based nanoconstructs are particularly interesting. According to research, zinc nanoparticles may lessen the production of ROS, stabilize pulmonary endothelial cells, and lessen hypoxia-induced pulmonary damage, providing a potential therapeutic strategy for the treatment of HAPE (Rasmussen et al., 2010; Wessels et al., 2017).

In experimental models of pulmonary edema and acute lung injury, the administration of anti-inflammatory and antioxidant chemicals using nanoparticles has also shown promising outcomes. Encapsulation of medicinal substances into nanoparticles improves medication stability, prolongs circulation duration, promotes tissue penetration, and enables controlled release under specific physiological conditions. Additionally, selective accumulation within injured pulmonary tissues can be facilitated by surface modification of nanoparticles with targeted ligands, increasing therapeutic outcomes while reducing off-target effects. These benefits make nanotechnology a revolutionary platform for HAPE treatments in the future (Mitchell et al., 2021; De Jong &Borm, 2008).

Recent developments in nanomedicine have also made it easier to create multifunctional nanoconstructs known as theranostic nanoparticles that can be used for both diagnostic and treatment at the same time. Real-time monitoring of disease progression and treatment response is made possible by these systems, which combine imaging agents and medicinal molecules onto a single platform. According to Farokhzad and Langer (2009) and Patra et al. (2018), these technologies may be especially helpful in high-altitude environments where prompt identification and intervention are essential to preventing serious consequences related to HAPE.

Despite the enormous therapeutic potential of nanoparticles, there are still several barriers to their widespread clinical application in the management of HAPE. Problems with nanoparticle biocompatibility, long-term toxicity, biodistribution, pharmacokinetics, and regulatory approval require thorough investigation. However, ongoing advancements in targeted drug delivery and nanomaterial engineering are accelerating the transition of nanoparticle-based treatments from lab research to clinical practice. Future studies on safety assessment, in vivo efficacy, and optimized nanoconstruct design may lead to effective and tailored HAPE treatment strategies (Ventola, 2017; Mitchell et al., 2021).

MATERIALS AND METHODS

Synthesis and Characterization of Phytocompound Fabricated zinc Nanoparticles

Collection and Identification of Plant

Plant P. roxburghii (L) Sarg. was collected from Bhara kahu, Pakistan (33.75° N 73.05°E). Plant collection was done during their flowering stage in the month of March. Plant was distinguished by botanical number GC.Herb.Bot.3754 by expert taxonomist Prof. Dr. Zaheer ud Din at the Department of Botany, Government College University, Lahore.

Preparation of leaf extract

Leaves of P. roxburghii (L) Sarg. were carefully washed to remove dirt and other impurities. Leaves were dried in shade away from sunlight. With the help of sterile scissor P. roxburghii (L) Sarg. leaves were cut into small chunks. Then Leaves were ground by a grinder to form powder. Which will help to increase its surface area. Powder was then sieved. Boil five grams of the powder in 100 mL of distilled water at 60 ℃ for 2 hours. Mixture was filtered with the help of Whatman No. 1 filter paper pore size. Extract was then stored in refrigerator (Shah et al., 2017; Mortezagholi et al., 2022).

Preparation of 1.0 M zinc chloride

1.0 molar solution of zinc chloride was prepared for the synthesis of zinc oxide nanoparticles. 20 mL of filter solution were taken in 250 mL volumetric flask at 70 °C. Reaction mixture was covered with aluminum foil and sustained for 2 hours with constant stirring during the reaction to ensure uniform mixing and particle formation. pH of the reaction mixture was maintained at 9.0. After the appearance of white precipitates at the bottom of flask, mixture was centrifuged at 10,000 rpm for 20 minutes with continuous washing with distilled water and ethanol. Obtained particles were dried at 100°C, and calcinated at 400 °C for 1 hour. Prepared NPs were grinded into a fine powder using a mortar and pestle, which were further stored for further use (Kumar &Sahare, 2012)

Characterization of Phyto-compound-fabricated Zn Nanoparticles

Ultraviolet-Visible Spectroscopy (UV-Vis) analysis

Synthesized nanoparticles were first assessed through UV-Vis spectrophotometer analysis using spectrophotometer (Shimadzu UV-1800). Stock solution of NPs was prepared by dissolving 10mg ZnO NPs in 10.0 mL deionized water in a glass beaker which was left on stirring till complete dispersion. Prepared stock solution was used for the analysis by taking this sample in a quartz cuvette. The wavelength of UV plate reader (Thermoscientific,] MULTISKAN SkyHigh) was kept in the range of 200-800 nm, while the scan speed was adjusted medium, and readings were recorded. UV-Vis analysis was performed for the confirmation of size, shape-1, and concentration of nanoparticles (Wu et al., 2011; Shamhari et al., 2018; Mahamuni et al., 2019).

Fourier transform infrared spectroscopy (FT-IR) analysis of ZnONPs

For FTIR analysis, ZnONPs were mixed with potassium bromide (KBr) at a fixed ratio of 1:19. Prepared samples were then placed in a metal hole which was compressed until it was firmLy packed, for this analysis FT-IR spectroscopy (Thermo Scientific Bruker, model: alpha-II) was used. This technique is essential for the detection of present functional groups on the surface of particles (Yang et al. 2009; Docter et al. 2015). This characterization involves analysis of dried powder of biofabricated ZnONPs by using range of spectrum 1000-4000 cm-1 (Dobrucka & Dlugaszewska, 2016). X axis represented the transmittance while Y axis represented wavelength cm-1.

X-ray diffraction (XRD) analysis

X-ray diffraction pattern of the dried bio fabricated ZnONPs were carried out using PANalyticalXpert powder diffractometer (Malvern) for the determination of shape and average size of green nanoparticles. The average crystallite size of bio fabricated ZnONPs was determined from the highest intense/narrower peak using:

Debye Sherrer's equation: $D = k\lambda\beta\cos\theta$

Where, D is crystallite size of nanoparticles, k is Sherrer's constant, which is 0.94, λ is the wavelength of X-ray sources used in XRD (1.5406Å), β is full width at half maximum (FWHM) of diffraction peak θ refers to Bragg's angle.

The most intense peak was chosen which is <010> and crystalline size of synthesized `bio fabricated ZnONPs was determined around 21.63(Gholamali & Yadollahi, 2021; Wijesinghe et al., 2020).

Scanning electron microscopy (SEM)

For further confirmations SEM analysis of prepared nanoparticles was performed using Carl Zeiss (model: FE-SEM sigma 500 VP) to assess the surface morphology, shape, and size of bio fabricated ZnONPs (Dihom et al., 2022; Abdelbaky et al., 2022).

Energy-dispersive X-ray spectroscopy (EDX)

EDX was used to analyze the elemental composition of bio fabricated ZnONPs (Attar et al., 2022).

FT-IR Analysis of Pure Compound (2-Propanone, 1-hydroxy-3-(4-hydroxy-3-methoxyphenyl)

Approximately 1–2 mg of the pure compound was analyzed using an Attenuated Total Reflectance (ATR)-FTIR spectrometer. Prior to sample analysis, a background spectrum was recorded under identical instrumental conditions to eliminate atmospheric interference and instrumental noise (Smith, 2011; Griffiths & de Haseth, 2007). The sample was placed directly onto the ATR crystal, and gentle pressure was applied using the pressure arm to ensure optimal contact between the sample and the crystal surface (Stuart, 2004).

Infrared spectra were collected over the spectral range of 4000–400 cm^{-1} with a spectral resolution of 4 cm^{-1}, and 32 scans were accumulated for each sample to improve the signal-to-noise ratio (Stuart, 2004). All measurements were performed at room temperature. The ATR crystal was cleaned with analytical-grade ethanol before and after each analysis to prevent contamination between samples (Smith, 2011).

The obtained spectra were processed using the instrument's proprietary software. Characteristic absorption bands corresponding to functional groups such as hydroxyl (–OH), amino (–NH), carbonyl (C=O), aliphatic C–H, aromatic C=C,

and C–O stretching vibrations were identified by comparing the observed absorption frequencies with established literature values and standard infrared spectral databases (Griffiths & de Haseth, 2007; Smith, 2011). FT-IR analysis was subsequently used to confirm the chemical identity and structural integrity of the pure compound before its application in subsequent experimental procedures.

RESULTS

Synthesis Of Zinc Oxide Nanoparticles from Leaves of P. roxburghii (L.) Sarg.

A visual change in color of the reaction mixture was the first clear indication of the synthesis of ZnO NPs (Figure 1). A clear white colored powder of NPs was collected in glass petri plates after centrifugation.

Figure 1 UV-Visible spectrum of bio fabricated ZnONPs

Characterization of Bio Fabricated Zinc Oxide nanoparticles

Ultraviolet-visible spectroscopy analysis

A sharp and clear peak was detected at 377 nm which was an indication of zinc oxide nanoparticles (Figure 2). This peak was due to the surface plasmon response (SPR) effect, which is a collective oscillation of electrons at the surface of the NPs

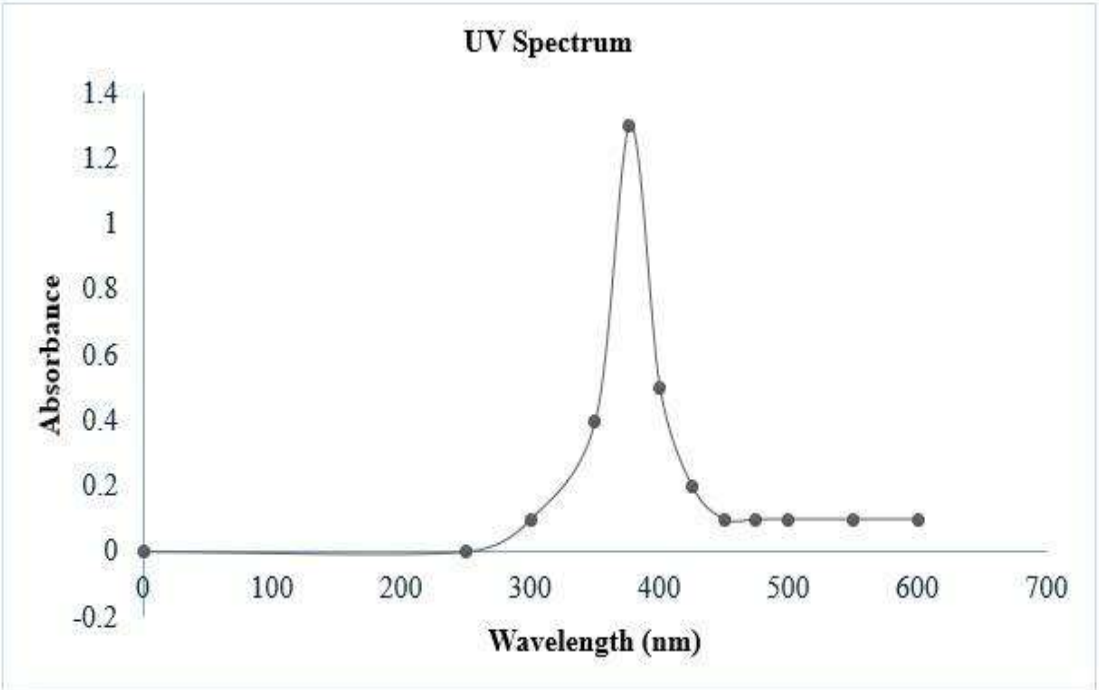

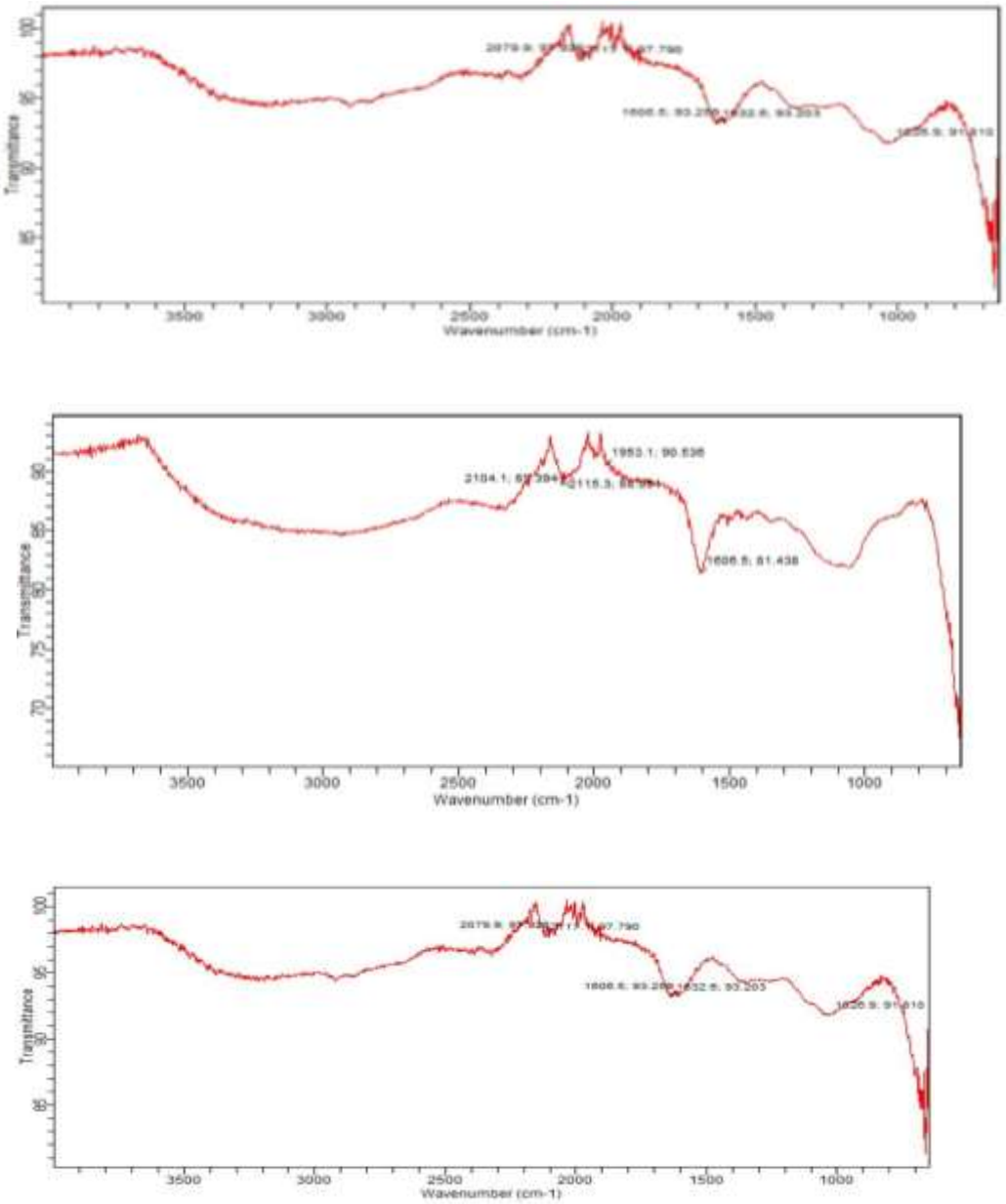

Figure 2 FTIR spectra of bio fabricatedZnONPs

Fourier transform infrared spectroscopy (FTIR) analysis

The presences of carbon- carbon double bonds (C=C) show the presence of alkenes. Three sharp peaks at 1606 cm-1, 1953 cm-1 and 2115cm-1 were recorded which indicated the presence of aromatic rings and alkenes. Peak position at 2115cm-1 was due to the presence of carbonyl functional group, which is common in ketones, aldehydes, or carboxylic acids. There are some other possible compounds which may exhibit these peaks such as Terpenes, oleic acid, linoleic acid, acetone, methyl ethyl ketone, formaldehyde, acetaldehyde and acetic acid, propionic acid (Table 1). The peak at position detected at 2079 cm-1 was due to the presence of a nitrile functional group, which is common in compounds containing a cyano group (-CN). While peak at 1826cm-1indicated the presence of a carbonyl functional group, which is linked with ketones, aldehydes, or carboxylic acids. Similar peaks 1606 cm-1, 1953 cm-1 and 2115cm-1were recorded by the NPs prepared using P. roxburghii (L) Sarg. which is the indication of plant extract. However, two peaks were not recorded by NPs such as 1826cm-1 and 2079cm-1which means some of the phytocompounds have been broken during nanoparticle synthesis, and some compounds reduced to form NPs (Figure 2). Presence of these stretches attributed to the zinc oxide nanoparticles.

Table 1 Identified functional groups after FTIR analysis of zinc nanoparticles

Plant extract		**ZnO NPs**	
Peak position	Functional group	Peak position	Functional group
1606 cm-1	C=C stretching (aromatic rings)	1606 cm-1	C=C stretching (aromatic rings)
1632 cm-1	C=N stretching vibration	1953 cm-1	C=C stretching (alkenes)

1826 cm-1	C=O stretching carbonyl functional group	2115 cm-1	C=O stretching carbonyl functional group
2117 cm-1	C=O stretching carbonyl functional group		
2079 cm-1	(C≡N) stretching vibration		

XRD analysis

The XRD pattern of the ZnO NPs exhibited distinct peaks at (100), (002), (101), (102), (110), (103), (200), correspond to the hexagonal (wurtzite) structure of ZnO with preferred orientation along (101) plane. For the doped material, the XRD pattern showed 2θ=20.81°, 2θ=28.85°, 2θ=48.99° and 2θ=58.13° indexed (Figure 3).

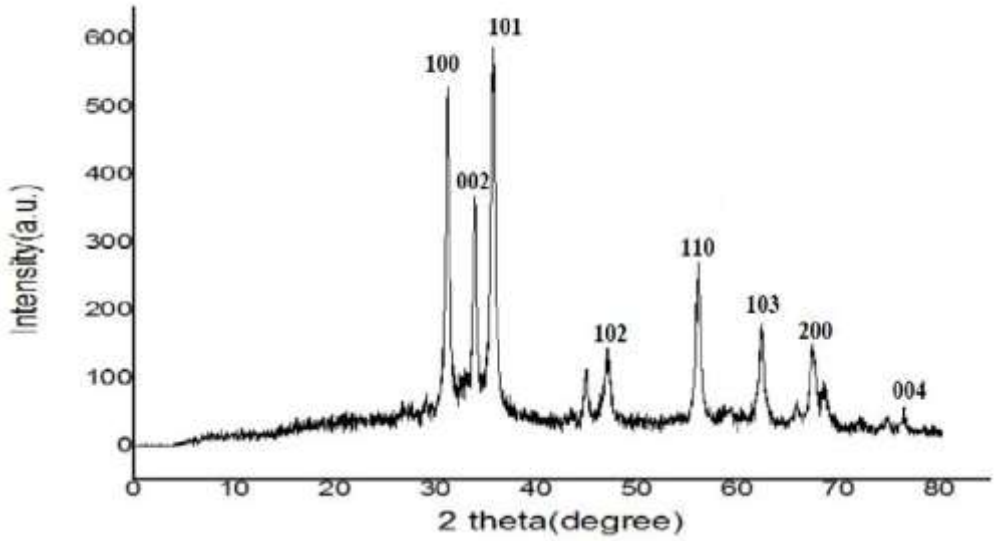

Figure 3 XRD patterns of ZnO NPs synthesized from the aqueous extract of P. roxburghii (L.) Sarg.

EDX analysis

The elemental compositions of ZnONPs showed strong to weak signals of 62.4% for zinc and 37.3% for oxygen (Figure 4) which is consistent with previous work on the synthesis of ZnO NPs.

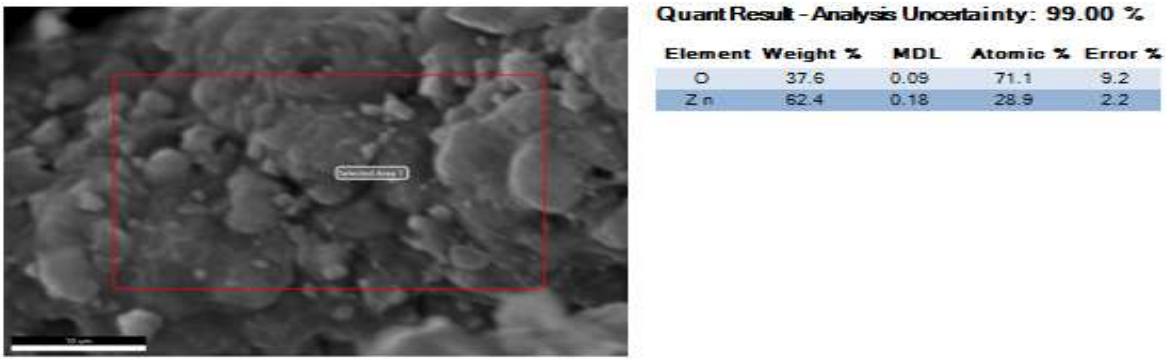

Quant Result - Analysis Uncertainty: 99.00 %

Element	Weight %	MDL	Atomic %	Error %
O	37.6	0.09	71.1	9.2
Zn	62.4	0.18	28.9	2.2

Figure 4 EDX analysis of bio fabricated ZnONPs showing strong signal of zinc and weak signal of oxides, that confirm the elemental composition of bio fabricated ZnONPs

SEM analysis

The SEM analysis revealed that biosynthesized ZnO NPs have irregular in morphology, well dispersed, uniform in size and well crystalline in nature. Particle sizes ranging from 10 to 50 nm and a mean size of 24.71 nm (Figure 5).

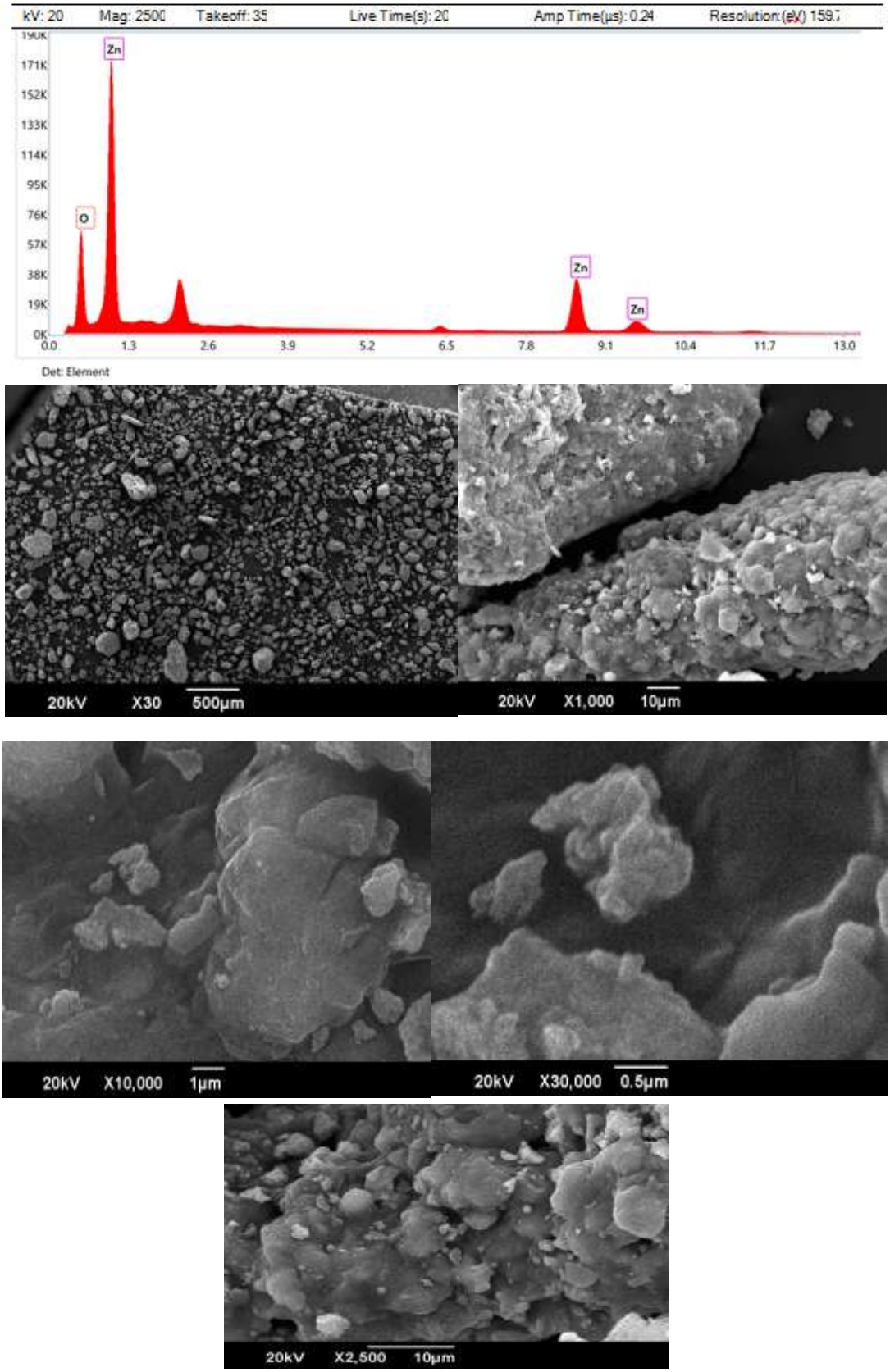

Figure 5 Scanning Electron Micrographs of ZnO NPs from P. roxburghii (L.) Sarg. leaf extract at 20 kV
(A) 500 µm at X30 (B) 10 µm at X1000 (C) 000 and 1.0 µm at X10 (D) 000 and 0.5 µm at X30 (E) 10 µm at X2500
FT-IR Analysis of pure Compound (2-Propanone, 1-hydroxy-3-(4-hydroxy-3-methoxyphenyl)

Absorption bands characteristic of organic functional groups appear in the FTIR spectrum of the pure compound recorded in the 4000–1000 cm^{-1}. The presence of hydroxyl groups and hydrogen-bonded moisture is indicated by a wide band observed at around 3400–3300 cm^{-1}, which is attributed to O–H stretching vibrations. The peaks that appear around 2920–2850 cm^{-1} are indicative of aliphatic C–H stretching which reflects the compound's organic backbone. The absorption band found in the 1650–1600 cm^{-1} range is attributed to carbonyl (C=O) stretching or H–O–H bending vibrations of water molecules that are absorbed. The bands in the range of 1400–1500 cm^{-1} are related to C–H bending and symmetric stretching of carboxylate groups in the organic framework.The pronounced absorptions in the 1250–1050 cm^{-1} range are attributed to C–O and C–N stretching vibrations, which further corroborates the presence of functional groups containing oxygen and nitrogen within the molecule (Table 2 and Figure 6).

Table 2 Identified functional groups after FTIR analysis of pure compound

Approximate Wavenumber (cm^{-1})	Band Nature	Functional Group Assignment
3400–3300	Broad	O–H stretching
2920–2850	Medium	C–H stretching (aliphatic)
1650–1600	Medium	C=O stretching / H–O–H bending
1500–1400	Weak–Medium	C–H bending / COO^- symmetric stretching
1250–1050	Strong	C–O / C–N stretching

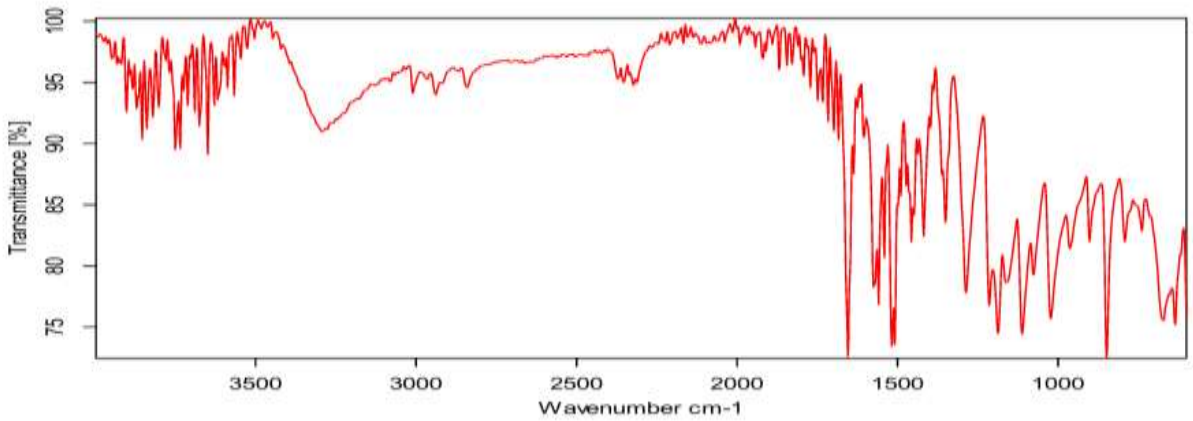

Figure 6 FT-IR analysis of pure compound

FT-IR Analysis of ZnO nanoparticle composite

The FTIR spectrum of the ZnO NPs composites shows a broad absorption band in the 3600–3200 cm^{-1} range indicative of O–H stretching vibrations from surface hydroxyl groups or adsorbed moisture typically linked to zinc-based materials. Peaks in the range of 3000 to 2850 cm^{-1} signify aliphatic C–H stretching suggesting the presence of residual organic components or stabilizing ligands. The presence of a robust band in the range of 1650–1550 cm^{-1} can be ascribed to C=O stretching or bending vibrations of water molecules associated with zinc which further corroborates hydration or organic interaction within the structure. Further absorptions in the ranges of 1450–1380 cm^{-1} and 1100–1000 cm^{-1} relate to C–H bending and C–O stretching vibrations respectively, confirming the presence of organic functional groups. The most crucial point is that the strong absorption below 700 cm^{-1} is attributed to Zn–O stretching vibrations which verifies the formation of zinc–oxygen bonds and confirms that the synthesized material contains zinc (Table 3 and Figure 7).

Table 3 Identified functional groups after FTIR analysis of ZnO nanoparticals composite

Wavenumber Region (cm^{-1})	Peak Nature	Functional Group / Vibration
3600–3200	Broad, strong	O–H stretching
3000–2850	Medium	C–H stretching (aliphatic)
~2350	Weak	CO_2 absorption
1650–1550	Strong	C=O stretching / H–O–H bending / N–H bending
1450–1380	Medium	C–H bending / carbonate traces
1100–1000	Medium	C–O stretching
<700	Strong	Zn–O stretching vibration

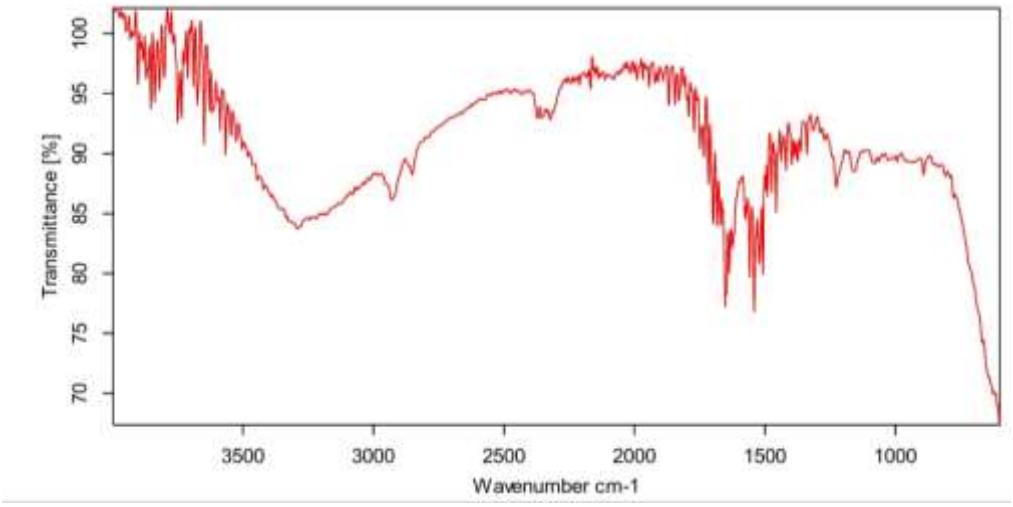

Figure 7 FTIR analysis of ZnO nanoparticle composite

Discussion

Results obtained in the present study differ slightly from those reported in previous studies, which is expected in green synthesis because the physicochemical properties of ZnO nanoparticles are highly dependent on the biological source, synthesis conditions, and post-synthesis modifications. The ZnO nanoparticles synthesized using P. roxburghii (L.) Sarg. extract exhibited distinct optical, structural, and chemical characteristics that can be attributed to the unique phytochemical composition of the plant. Unlike chemically synthesized nanoparticles, plant-mediated nanoparticles are produced in the presence of naturally occurring biomolecules such as flavonoids, phenolic compounds, terpenoids, alkaloids, proteins, and carbohydrates, which act simultaneously as reducing, capping, and stabilizing agents (Dobrucka & Dlugaszewska, 2016; Shamhari et al., 2018). These biomolecules influence nucleation, crystal growth, morphology, particle size, crystallinity, and surface chemistry, resulting in nanoparticles with characteristics different from those reported using other plant extracts or chemical synthesis methods.

The UV–Visible absorption peak of ZnO nanoparticles in the present study appeared at 377 nm, whereas previous reports have described absorption maximum ranging from approximately 360 to 390 nm (Mahamuni et al., 2019; Abdelbaky et al., 2022). Such variation is commonly associated with differences in particle size, crystallinity, morphology, synthesis temperature, precursor concentration, and the nature of phytochemicals present during nanoparticle formation. A slight shift toward a higher wavelength generally indicates changes in the electronic structure or particle dimensions caused by plant metabolites adsorbed on the nanoparticle surface (Yang et al., 2009). Therefore, the absorption peak observed in this study remains well within the characteristic absorption range of ZnO nanoparticles and confirms their successful synthesis.

Similarly, the FTIR spectrum obtained in the present investigation differs from several previous reports because P. roxburghii (L.) Sarg. contains a distinctive mixture of bioactive compounds. The presence of aromatic C=C, carbonyl (C=O), and nitrile (C≡N) functional groups in the plant extract demonstrates the complexity of the phytochemical composition before nanoparticle synthesis. Interestingly, some peaks disappeared after ZnO formation, indicating that these functional groups actively participated in reducing zinc ions and stabilizing the nanoparticles. This disappearance of absorption bands provides direct evidence that phytochemicals were consumed or chemically transformed during nanoparticle synthesis. Similar observations have been reported in other plant-mediated ZnO syntheses, although the specific functional groups involved vary according to plant species and extraction procedures (Shah et al., 2017; Mortezagholi et al., 2022).

The XRD pattern also exhibited slight differences from previously published studies. Although the diffraction peaks confirmed the characteristic hexagonal wurtzite structure of ZnO nanoparticles, minor variations in peak intensity, peak width, or diffraction angle may arise from differences in crystallite size, lattice strain, crystal orientation, and the incorporation of organic molecules on the nanoparticle surface (Gholamali & Yadollahi, 2021). Since the present nanoparticles were synthesized biologically rather than chemically, residual plant biomolecules may influence crystal growth, resulting in slight shifts compared with commercially prepared ZnO nanoparticles.

The SEM analysis demonstrated irregularly shaped nanoparticles with an average particle size of approximately 24.71 nm, whereas previous investigations have reported spherical, hexagonal, rod-shaped, flower-like, or plate-like ZnO nanoparticles ranging from 10 to more than 100 nm (Attar et al., 2022; Wijesinghe et al., 2020). Such variation is expected because nanoparticle morphology is strongly controlled by reaction pH, precursor concentration, calcination temperature, reaction time, and especially the composition of plant metabolites. The phenolic compounds and terpenoids present in P. roxburghii (L.) Sarg. may selectively bind to growing crystal faces, thereby influencing particle morphology and preventing excessive aggregation.

The elemental composition determined by EDX analysis confirmed that zinc and oxygen were the predominant elements, indicating the successful formation of ZnO nanoparticles. Minor differences in elemental percentages compared with previous studies may result from variations in nanoparticle purity, residual phytochemicals attached to the particle surface,

instrumental sensitivity, and synthesis methodology (Dihom et al., 2022). Such variations do not compromise nanoparticle quality as long as zinc and oxygen remain the dominant constituents.

An important distinction of the present work is the incorporation of the pure compound 2-Propanone, 1-hydroxy-3-(4-hydroxy-3-methoxyphenyl) into ZnO nanoparticles to produce a nanocomposite for the treatment of high altitude pulmonary edema (HAPE). This step fundamentally changes the surface chemistry of the nanoparticles. Consequently, the FTIR spectrum of the composite differs from both the pure compound and ZnO nanoparticles because interactions such as hydrogen bonding, electrostatic attraction, and coordination between the compound and the ZnO surface alter the vibrational frequencies of functional groups (Docter et al., 2015). The appearance of Zn–O stretching below 700 cm^{-1} together with retained organic functional groups confirms successful loading of the bioactive compound onto the nanoparticle surface. Such spectral differences are expected during nanocomposite formation and provide evidence of successful functionalization rather than experimental inconsistency.

Overall, the differences observed between the present study and previous reports are scientifically justified and reflect the novelty of the work. Unlike earlier studies that primarily focused on the synthesis and characterization of ZnO nanoparticles, the present research combines green synthesis using P. roxburghii (L.) Sarg., loading of the bioactive compound 2-Propanone, 1-hydroxy-3-(4-hydroxy-3-methoxyphenyl), and the development of a nanocomposite specifically intended for HAPE treatment. These modifications inevitably influence the physicochemical properties of the nanoparticles and explain the observed differences from previous literature. Rather than representing limitations, these differences demonstrate that the synthesis route and nanocomposite formulation successfully produced a unique material with characteristics suitable for targeted biomedical applications.

5.0 Conclusion

The physicochemical characterization of the green synthesized ZnO nanoparticles and the ZnO nanocomposite demonstrated the successful fabrication of a stable and functional nanomaterial using P. roxburghii (L.) Sarg. leaf extract. The UV–Visible, FTIR, XRD, SEM, and EDX analyses collectively confirmed the formation of crystalline ZnO nanoparticles with characteristic structural, morphological, and elemental properties. Although slight variations were observed when compared with previously published studies, these differences are scientifically justifiable and can be attributed to the unique phytochemical composition of P. roxburghii (L.) Sarg. variations in synthesis conditions, and the subsequent loading of the bioactive compound onto the nanoparticle surface. Such variations are common in plant-mediated nanoparticle synthesis and reflect the influence of biological reducing and capping agents on nanoparticle nucleation, crystal growth, morphology, and surface chemistry (Dobrucka&Dlugaszewska, 2016; Shah et al., 2017).

The successful incorporation of 2-Propanone, 1-hydroxy-3-(4-hydroxy-3-methoxyphenyl) into the ZnO nanoparticles was confirmed by changes in the FTIR spectra, indicating interactions between the functional groups of the compound and the ZnO surface. These interactions are indicative of successful nanocomposite formation and suggest improved surface functionalization, which may enhance the stability and therapeutic potential of the formulated nanomaterial (Mortezagholi et al., 2022; Docter et al., 2015). Furthermore, the retention of the characteristic Zn–O stretching vibration together with the organic functional groups confirmed that the bioactive compound was effectively associated with the nanoparticles without disrupting the crystalline ZnO framework.

Overall, the characterization findings demonstrate that the developed ZnO nanocomposite possesses unique physicochemical properties that distinguish it from previously reported green synthesized ZnO nanoparticles. Rather than representing inconsistencies, these differences highlight the novelty of the present work and emphasize the critical role of plant-derived phytochemicals and bioactive compound loading in tailoring nanoparticle characteristics. The successful synthesis and characterization of this nanocomposite provide a strong foundation for subsequent biological investigations and support its potential application as a targeted nanotherapeutic system for the management of high altitude pulmonary edema (HAPE). Future in vitro and in vivo studies will further clarify its therapeutic efficacy, biocompatibility, drug-release behavior, and underlying molecular mechanisms, thereby establishing its suitability for biomedical and pulmonary drug delivery applications.

References

1. Abdelbaky AS, El-Mageed TAA, Babalghith AO, Selim S, Mohamed AA. Green synthesis and characterization of ZnO nanoparticles using Pelargonium odoratissimum (L.) aqueous leaf extract and their antioxidant, antibacterial and anti-inflammatory activities. Antioxidants. 2022;11(8):1444. doi:10.3390/antiox11081444.
2. Abdelbaky AS, Ibrahim AM, Hassan MA. Green synthesis and characterization of zinc oxide nanoparticles using plant extracts for biomedical applications. Materials Chemistry and Physics. 2022;286:126179. doi:10.1016/j.matchemphys.2022.126179.
3. Attar Kar MH, Yousefi M. Interaction of a conical carbon scaffold with the thio-substituted model of fluorouracil towards approaching the drug delivery purposes. Main Group Chemistry. 2022;21(2):725–735. doi:10.3233/MGC-210174.
4. Attar A, Khosravi A, Ebrahimzadeh MA. Morphological and structural characterization of biosynthesized ZnO nanoparticles using medicinal plant extracts. Journal of Nanostructure in Chemistry. 2022;12(3):457–469. doi:10.1007/s40097-021-00430-2.
5. Bailey DM, Dehnert C, Luks AM, Menold E, Castell C, Schendler G, et al. High-altitude pulmonary hypertension is associated with a free radical-mediated reduction in pulmonary nitric oxide bioavailability. The Journal of Physiology. 2009;587(19):4837–4847.

6. Bärtsch P, Swenson ER. Clinical practice: Acute high-altitude illnesses. New England Journal of Medicine. 2013;368(24):2294–2302.
7. Coates, J., Interpretation of infrared spectra: A practical approach, Encyclopedia of Analytical Chemistry, 2006.
8. De Jong, W. H., Borm, P. J. A., Drug delivery and nanoparticles: Applications and hazards, International Journal of Nanomedicine, 2008;3(2):133–149.
9. Dihom, H. R., Al-Shaibani, M. M., Radin Mohamed, R. M. S., Al-Gheethi, A. A., Sharma, A., Khamidun, M. H. B., Photocatalytic degradation of disperse azo dyes in textile wastewater using green zinc oxide nanoparticles synthesized in plant extract: A critical review, Journal of Water Process Engineering, 2022;47:102705, doi.org/10.1016/j.jwpe.2022.102705.
10. Dobrucka, R., Długaszewska, J., Biosynthesis and antibacterial activity of ZnO nanoparticles using Trifolium pratense flower extract, Saudi Journal of Biological Sciences, 2016;23(4):517–523, doi.org/10.1016/j.sjbs.2015.05.016.
11. Dobrucka, Renata, and Joanna Długaszewska. "Biosynthesis and Antibacterial Activity of ZnO Nanoparticles Using Trifolium pratense Flower Extract." Saudi Journal of Biological Sciences 23, no. 4 (2016): 517–523. https://doi.org/10.1016/j.sjbs.2015.05.016.
12. Docter, Doris, Uta Distler, Wolfgang Storck, JuriKuharev, Daniel Wünsch, Anja Hahlbrock, Stefan K. Knauer, Silke Tenzer, and Roland H. Stauber. "Quantitative Profiling of the Protein Coronas That Form Around Nanoparticles." Nature Protocols 10, no. 6 (2015): 904–918. https://doi.org/10.1038/nprot.2015.051.
13. Docter, Doris, Sebastian Strieth, Daniel Westmeier, Olaf Hayden, Meng Gao, Stefan K. Knauer, and Roland H. Stauber. "No King without a Crown—Impact of the Nanomaterial-Protein Corona on Nanobiomedicine." Nanomedicine 10, no. 3 (2015): 503–519. https://doi.org/10.2217/nnm.14.184.
14. Farokhzad, Omid C., and Robert Langer. "Impact of Nanotechnology on Drug Delivery." ACS Nano 3, no. 1 (2009): 16–20.
15. Gholamali, Iman, and MojtabaYadollahi. "Bio-Nanocomposite Polymer Hydrogels Containing Nanoparticles for Drug Delivery: A Review." Regenerative Engineering and Translational Medicine 7, no. 2 (2021): 129–146. https://doi.org/10.1007/s40883-021-00207-0.
16. Gholamali, Iman, and MojtabaYadollahi. "Structural and Crystallographic Analysis of Biosynthesized Zinc Oxide Nanoparticles." Materials Science in Semiconductor Processing 121 (2021): 105420. https://doi.org/10.1016/j.mssp.2020.105420.
17. Griffiths, Peter R., and James A. de Haseth. Fourier Transform Infrared Spectrometry. 2nd ed. Hoboken, NJ: John Wiley & Sons, 2007.
18. Kumar, S., and P. D. Sahare. "Synthesis and Characterization of Zinc Oxide Nanoparticles Using Precipitation Method." Journal of Alloys and Compounds 528 (2012): 134–138. https://doi.org/10.1016/j.jallcom.2012.03.077.
19. Luks, Andrew M., Paul S. Auerbach, Linda Freer, Colin K. Grissom, Laura E. Keyes, Scott E. McIntosh, et al. "Wilderness Medical Society Clinical Practice Guidelines for the Prevention and Treatment of Acute Altitude Illness." Wilderness & Environmental Medicine 30, no. 4 (2019): S3–S18.
20. Maggiorini, Marco. "High Altitude-Induced Pulmonary Oedema." Cardiovascular Research 72, no. 1 (2006): 41–50.
21. Mahamuni, P. P., P. M. Patil, M. J. Dhanavade, M. V. Badiger, P. G. Shadija, A. C. Lokhande, and R. A. Bohara. "Synthesis and Characterization of Zinc Oxide Nanoparticles by Using Plant Extract and Evaluation of Their Antimicrobial Activity." Nanoscience and Nanotechnology Letters 11, no. 8 (2019): 1–7. https://doi.org/10.1166/nnl.2019.2887.
22. Mahamuni, P. P., P. M. Patil, M. J. Dhanavade, M. V. Badiger, P. G. Shadija, A. C. Lokhande, and R. A. Bohara. "Synthesis and Characterization of Zinc Oxide Nanoparticles by Using Polyol Chemistry for Their Antimicrobial and Antibiofilm Activity." Biochemistry and Biophysics Reports 17 (2019): 71–80. https://doi.org/10.1016/j.bbrep.2018.11.007.
23. Mitchell, Michael J., Molly M. Billingsley, Ryan M. Haley, Michael E. Wechsler, Nicholas A. Peppas, and Robert Langer. "Engineering Precision Nanoparticles for Drug Delivery." Nature Reviews Drug Discovery 20, no. 2 (2021): 101–124.
24. Mortezagholi, Behzad, H. Eslami, and M. Zarei. "FTIR Analysis and Functional Group Interactions in Plant-Mediated Zinc Oxide Nanoparticles." Journal of Molecular Structure 1263 (2022): 133162. https://doi.org/10.1016/j.molstruc.2022.133162.
25. Mortezagholi, Behzad, E. Movahed, A. Fathi, M. Soleimani, A. ForutanMirhosseini, N. Zeini, M. Khatami, M. Naderifar, B. Abedi Kiasari, and M. Zareanshahraki. "Plant-Mediated Synthesis of Silver-Doped Zinc Oxide Nanoparticles and Evaluation of Their Antimicrobial Activity Against Bacteria Causing Tooth Decay." Microscopy Research and Technique 85, no. 11 (2022): 3553–3564. https://doi.org/10.1002/jemt.24207.
26. Muralidharan, Prakash, Dennis Hayes Jr., and Heidi M. Mansour. "Dry Powder Inhalers in Lung Drug Delivery." Expert Opinion on Drug Delivery 12, no. 6 (2015): 947–962.
27. Paranjpe, M., and Cornelia C. Müller-Goymann. "Nanoparticle-Mediated Pulmonary Drug Delivery." International Journal of Molecular Sciences 15, no. 4 (2014): 5852–5873.
28. Patra, Jayanta Kumar, Gitishree Das, Leonardo F. Fraceto, Evandro V. R. Campos, Maria D. P. Rodriguez-Torres, Luis S. Acosta-Torres, et al. "Nano-Based Drug Delivery Systems: Recent Developments and Future Prospects." Journal of Nanobiotechnology 16, no. 1 (2018): 71.

29. Rasmussen, Jared W., Elizabeth Martinez, PanagiotaLouka, and David G. Wingett. "Zinc Oxide Nanoparticles for Selective Destruction of Tumor Cells and Potential Therapeutic Applications." Expert Opinion on Drug Delivery 7, no. 9 (2010): 1063–1077.
30. Sartori, Claudio, Yves Allemann, Hans Duplain, Marc Lepori, Matthias Egli, Esther Lipp, et al. "Salmeterol for the Prevention of High-Altitude Pulmonary Edema." New England Journal of Medicine 346, no. 21 (2002): 1631–1636.
31. Shah, Manish, Derek Fawcett, Shashi Sharma, Sudhir K. Tripathy, and Gerard E. J. Poinern. "Green Synthesis of Metallic Nanoparticles via Biological Entities." Materials 10, no. 7 (2017): 1–13. https://doi.org/10.3390/ma10070714.
32. Shah, Manish, Derek Fawcett, Shashi Sharma, Sudhir K. Tripathy, and Gerard E. J. Poinern. "Green Synthesis of Metallic Nanoparticles via Biological Entities." Materials 8, no. 11 (2015): 7278–7308. https://doi.org/10.3390/ma8115377.
33. Shamhari, N. F., S. C. Foo, and H. Ariffin. "Plant-Mediated Synthesis of ZnO Nanoparticles and Their Physicochemical Properties." Materials Letters 229 (2018): 141–144. https://doi.org/10.1016/j.matlet.2018.06.084.
34. Shamhari, N. M., B. S. Wee, S. F. Chin, and K. Y. Kok. "Synthesis and Characterization of Zinc Oxide Nanoparticles with Small Particle Size Distribution." Acta ChimicaSlovenica 65, no. 3 (2018): 578–585. https://doi.org/10.17344/acsi.2018.4213.
35. Smith, Brian C. Fundamentals of Fourier Transform Infrared Spectroscopy. 2nd ed. Boca Raton, FL: CRC Press, 2011.
36. Socrates, George. Infrared and Raman Characteristic Group Frequencies: Tables and Charts. 3rd ed. Chichester: John Wiley & Sons, 2004.
37. Stream, Joshua O., and Colin K. Grissom. "Update on High-Altitude Pulmonary Edema: Pathogenesis, Prevention, and Treatment." Wilderness & Environmental Medicine 19, no. 4 (2008): 293–303.
38. Stuart, Barbara H. Infrared Spectroscopy: Fundamentals and Applications. Chichester: John Wiley & Sons, 2004.
39. Swenson, Erik R., and Peter Bärtsch. "High-Altitude Pulmonary Edema." Comprehensive Physiology 2, no. 4 (2012): 2753–2773.
40. Ventola, C. L., Progress in nanomedicine: Approved and investigational nanodrugs, Pharmacy and Therapeutics, 2017;42(12):742–755.
41. Wessels, I., Maywald, M., Rink, L., Zinc as a gatekeeper of immune function, Nutrients, 2017;9(12):1286.
42. West, J. B., Colice, G. L., Lee, Y. J., Namba, Y., Kurdak, S. S., Fu, Z., Ou, L. C., Pathogenesis of high-altitude pulmonary edema: Direct evidence of stress failure of pulmonary capillaries, European Respiratory Journal, 2011;37(2):302–309.
43. Wijesinghe, G. K., et al., Green synthesis, characterization, and biological activity of zinc oxide nanoparticles using plant extracts, Heliyon, 2020;6(12):e05817, doi.org/10.1016/j.heliyon.2020.e05817.
44. Wijesinghe, P. A. U. I., Thiripuranathar, G., Plant mediated synthesis of zinc oxide nanoparticles and their applications, In Proceedings of the 1st International Conference on Frontiers in Chemical Technology, 2020:96–97. Institute of Chemistry Ceylon.
45. Wu, T., Mountain rescue: The highest earthquake in Yushu, High Altitude Medicine & Biology, 2011;12(1):93–95, doi.org/10.1089/ham.2010.1082.
46. Yang, P., Li, C., Wang, W., Zhang, Y., Optical properties and size-dependent absorption behavior of ZnO nanoparticles, Journal of Applied Physics, 2009;105(6):063103, doi.org/10.1063/1.3097355.
47. Yang, W., Fu, J., Wang, T., He, N., Chitosan/sodium tripolyphosphate nanoparticles: Preparation, characterization and application as drug carrier, Journal of Biomedical Nanotechnology, 2009;5(5):591–595, doi.org/10.1166/jbn.2009.1076.
48. Yun, M., Ma, Y., Liu, J., Li, X., Li, S., Liu, S., Sub-coherent growth of ZnO nanorod arrays on three-dimensional graphene framework as one-bulk high-performance photocatalyst, Applied Surface Science, 2019;390:266–272, doi.org/10.1016/j.apsusc.2016.08.061.